Room-temperature continuous-wave operation of GaInAsP/InP lateral-current-injection membrane laser bonded on Si substrate

2014 Appl. Phys. Express 7 072701

(http://iopscience.iop.org/1882-0786/7/7/072701)

Applied Physics Express 7, 072701 (2014)
http://dx.doi.org/10.7567/APEX.7.072701

Room-temperature continuous-wave operation of GaInAsP/InP lateral-current-injection membrane laser bonded on Si substrate

Daisuke Inoue[1*], Jieun Lee[1], Kyohei Doi[1], Takuo Hiratani[1], Yuki Atsuji[1], Tomohiro Amemiya[2], Nobuhiko Nishiyama[1], and Shigehisa Arai[1,2]

[1]*Department of Electrical and Electronic Engineering, Tokyo Institute of Technology, Meguro, Tokyo 152-8552, Japan*
[2]*Quantum Nanoelectronics Research Center, Tokyo Institute of Technology, Meguro, Tokyo 152-8552, Japan*
E-mail: inoue.d.ac@m.titech.ac.jp

Received May 4, 2014; accepted June 5, 2014; published online June 25, 2014

We successfully demonstrated room-temperature continuous-wave (RT-CW) operation of a lateral-current-injection (LCI) GaInAsP/InP membrane Fabry–Perot laser by benzocyclobutene (BCB) adhesive bonding on a Si substrate for the first time. Our results include, for example, a threshold current of 2.5 mA and an external differential quantum efficiency of 22% per facet were obtained for a stripe width of 0.7 μm and a cavity length of 350 μm. From measurements of the differential quantum efficiency as a function of the cavity length, an internal quantum efficiency of 75% and a waveguide loss of 42 cm^{-1} were obtained. © 2014 The Japan Society of Applied Physics

Optical interconnect technology is the most attractive solution for global wiring problems affecting LSI circuits.[1–3] The copper interconnections in global wire layers have bottlenecks due to signal delay and Joule heating and, in contrast to MOSFETs, these characteristics are not improved by the scaling law.[4] Recently, on-chip optical interconnections have been extensively investigated, as this technology can potentially overcome the abovementioned problems. In order to do so, on-chip optical devices are required to operate with ultralow power consumption, a small footprint, and easy integration. With regards to the energy cost of a light source in such an application, the available energy of the semiconductor laser was originally estimated to be 100 fJ/bit[5] and has recently been claimed to be significantly less. Several research groups have reported the development of ultralow-power-consumption semiconductor lasers such as vertical-cavity surface-emitting lasers (VCSELs)[6,7] and photonic crystal lasers.[8–10]

We have proposed semiconductor-membrane distributed feedback lasers (DFB) and demonstrated their low-threshold operation under room-temperature continuous-wave (RT-CW) optical pumping,[11–13] during which CW operation of up to 85 °C was obtained.[14] Since the membrane structure consists of a thin (100–200 nm) semiconductor core layer sandwiched between low-refractive-index dielectric cladding layers, the large refractive-index difference between the core and cladding layers leads to strong optical confinement in the semiconductor core layer. Therefore, the modal gain at a certain injection current level is enhanced by a factor of approximately three compared with that of conventional vertical-injection-type semiconductor lasers.[15,16] This will result in fewer instances of lower-threshold-current operation compared to conventional lasers with the same stripe width and cavity length.[12,13,17] Moreover, this design also leads to a large index-coupling coefficient for the grating, and realization of an ultralow-threshold-current DFB laser with an extremely short cavity length is therefore possible.

For the current-injection operation, we adopted a lateral-current-injection (LCI) structure[18] and obtained RT-CW operation of LCI lasers prepared on a semi-insulating InP substrate.[19] To prepare the membrane structure, we utilized the wafer bonding technique[15,20] using benzocyclobutene (BCB) as an intermediate layer. RT-CW operation of LCI-membrane (core thickness 220 nm) lasers prepared on an InP substrate was realized.[21] However, optical links consisting of LCI-membrane DFB lasers, low-loss waveguides, and compact/fast photodiodes on a Si substrate, while maintaining back-end process compatibility, will be attractive for integration with CMOS LSI circuits.

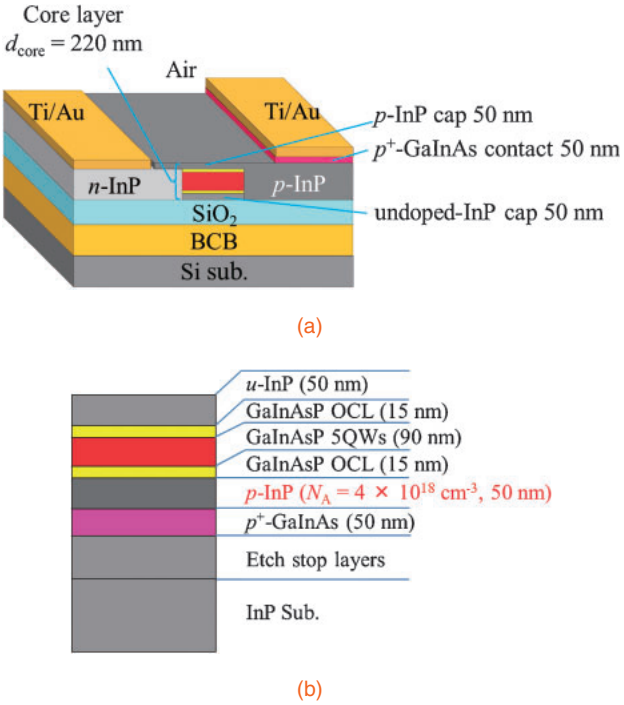

Fig. 1. (a) Schematic structure of a membrane laser prepared on a Si substrate and (b) the initial wafer structure.

In this letter, RT-CW operation of LCI-membrane Fabry–Perot (FP) lasers fabricated on a Si substrate is reported, and the internal quantum efficiency and waveguide loss are evaluated from the cavity length dependence of the differential quantum efficiency.

Figures 1(a) and 1(b) show the schematic structure of the fabricated device and initial wafer structure, respectively. The initial wafer consists of etch stop layers (300-nm-thick GaInAs and 100-nm-thick InP), a p^+-GaInAs contact layer (Be-doped, $N_A = 8 \times 10^{18}$ cm^{-3}, 50 nm), a p-InP layer (Be-doped, $N_A = 4 \times 10^{18}$ cm^{-3}, 50 nm), and five 1% compres-

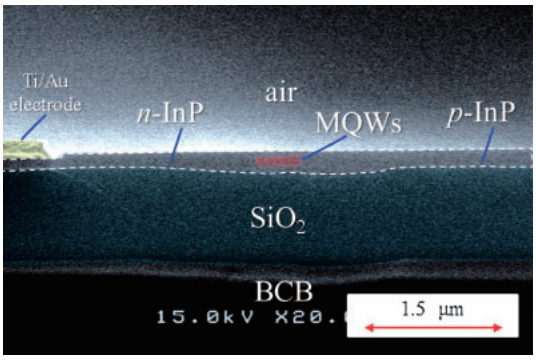

Fig. 2. Cross-sectional SEM image of the LCI-membrane laser.

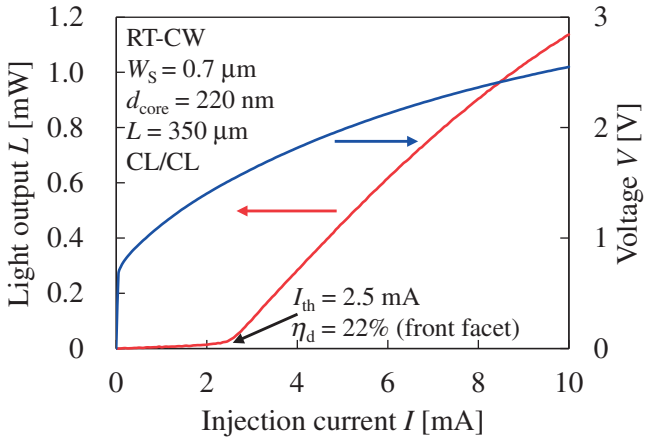

Fig. 3. Light output and voltage–current characteristics of an LCI-membrane FP laser with a cavity length of 350 μm.

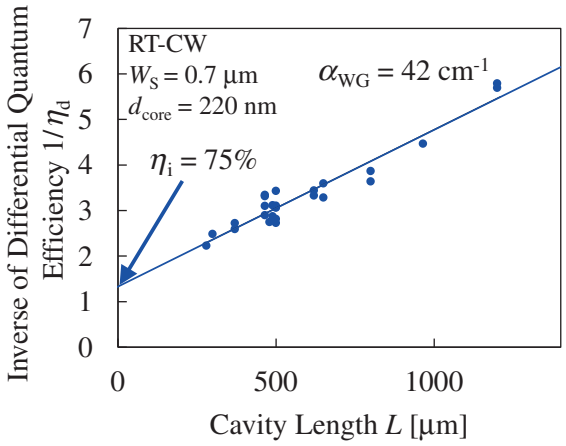

Fig. 4. Cavity length dependence of the inverse of the differential quantum efficiency of LCI-membrane FP lasers.

sively strained $Ga_{0.22}In_{0.78}As_{0.81}P_{0.19}$ quantum wells (undoped, 6 nm thick). These quantum wells have 0.15% tensile-strained $Ga_{0.26}In_{0.74}As_{0.49}P_{0.51}$ barriers (undoped, 10 nm thick) sandwiched by GaInAsP optical confinement layers (OCL; undoped, 15 nm thick). Therefore, the total thickness of the membrane core layer corresponds to 220 nm, and it is grown on an n-InP substrate using gas source molecular beam epitaxy (MBE).

The fabrication process of LCI-membrane lasers on a Si substrate is as follows. First, a lateral pn junction is formed to prepare the LCI structure using two-step organometallic vapor phase epitaxy (OMVPE) selective-area regrowth. A mesa stripe (covered with 7-μm-wide and 50-nm-thick SiO_2 masks) is formed by CH_4/H_2 reactive-ion etching (RIE), followed by n-InP (doping concentration, $N_D = 4 \times 10^{18}$ cm^{-3}) regrowth on both sides of the mesa stripes. Subsequently, one side of the n-InP layer is again etched in the same manner as previously mentioned, so as to leave the intended active region stripe width, and p-InP (doping concentration, $N_A = 4 \times 10^{18}$ cm^{-3}) is regrown.

Next, a 1-μm-thick SiO_2 film is deposited on the wafer through plasma-chemical-vapor-deposition (PCVD) and bonded upside-down onto the Si host substrate, on which a 2-μm-thick BCB is spin coated and pre-cured at a temperature of 210 °C in an N_2 atmosphere. These wafers are pressed under a pressure of approximately 25 kPa at 130 °C and the bonded wafer is hard-cured at 250 °C for 1 h in an N_2 atmosphere. After the wafer-bonding process, the InP substrate side and etch stop layers are removed with polishing and wet chemical etching, using selective etchants for GaInAs and InP. The revealed Be-doped contact layer is also removed by the selective etchant for GaInAs, in all areas apart from the p-electrode region. Finally, after removing the p-InP cap layer on the n-electrode region, Ti/Au electrodes are deposited on both the p^+-GaInAs contact layer and n-InP layer. Figure 2 shows a cross-sectional scanning-electron-microscopic (SEM) image of the fabricated LCI-membrane FP structure, confirming that the upper p-InP cap layer below the n-electrode has been removed.

The wafer then undergoes cleavage to form FP lasers with various cavity lengths, so as to measure light output characteristics and their dependences on cavity length. Figure 3 shows the light–current (L–I) and voltage–current (V–I) curves of a device with a cavity length, L, of 350 μm and a stripe width, W_s, of 0.7 μm under RT-CW conditions. A threshold current, I_{th}, of 2.5 mA (threshold current density, $J_{th} = 1100$ A/cm^2) and an external differential quantum efficiency, η_d, of 22% (front facet) were obtained. We obtained an output power of 1.1 mW at an injection current of 10 mA. This is the first RT-CW operation of an LCI-membrane FP laser bonded on a Si substrate. Because the light output measured from the rear facet was identical to that of the front facet, the differential quantum efficiency of this device was 44%.

Figure 4 shows the measured cavity length dependence of the inverse of the differential quantum efficiency, η_d. The relation between these two variables can be expressed by the following equation, assuming that the reflectivities of both facets are equal

$$\frac{1}{\eta_d} = \frac{1}{\eta_i}\left[1 + \frac{\alpha_{WG} L}{\ln(1/R)}\right], \quad (1)$$

where η_i denotes the internal quantum efficiency, R is the facet reflectivity, L is the cavity length, and α_{WG} is the waveguide loss. From linear extrapolation using Eq. (1), we obtained an η_i of 75% from a y-axis cut and an α_{WG} of 42 cm^{-1} from the slope of the linear fit. The internal quantum efficiency, η_i, of 75% is close to that of our one-step grown vertical injection lasers, as well as to the results for our LCI

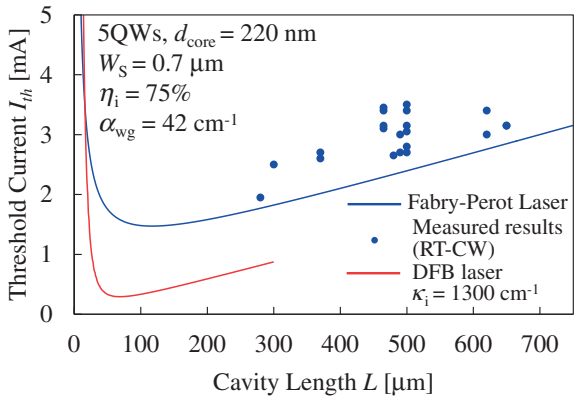

Fig. 5. Cavity length dependence of the threshold current for measured FP lasers and theoretical curves for FP lasers (blue line) and DFB lasers, with $\kappa_i = 1300\,\mathrm{cm}^{-1}$ (red line).

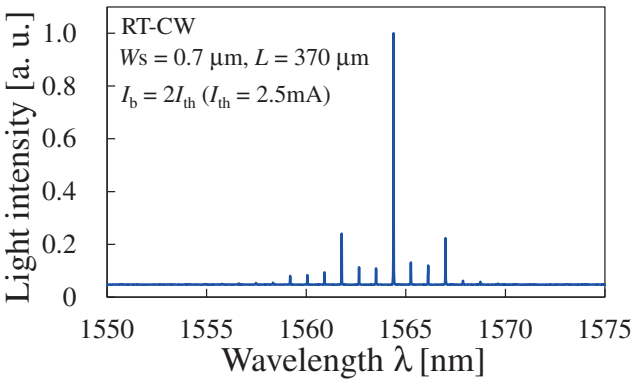

Fig. 6. Lasing spectrum of an LCI membrane FP laser with a cavity length of 370 μm and a stripe width of 0.7 μm.

lasers prepared on a semi-insulating InP substrate.[19] This indicates that nonradiative carrier recombinations at both the top and bottom surfaces of the membrane structure are almost negligible, which is attributed to 50-nm-thick InP cap layers as well as high-quality buried heterostructure interfaces prepared by two-step OMVPE regrowth. In addition, this high internal quantum efficiency indicates that there is minimal leakage current through the p-InP cap layer to the n-InP layer. However, the waveguide loss, α_{WG}, of $42\,\mathrm{cm}^{-1}$ is very large compared with our previously reported value ($5.1\,\mathrm{cm}^{-1}$) for LCI lasers on a semi-insulating InP substrate.[19] This may be attributed to scattering loss arising from the steps at the regrown interface between the mesa stripe and the InP cladding layers. Because the electric field is strongly confined in the thin semiconductor core, these steps induce a large scattering loss.

Figure 5 shows the theoretical calculations of the cavity length dependence of the threshold current for membrane FP lasers (blue solid line) and for membrane DFB lasers (red solid line), using the experimentally obtained values of $\eta_i = 75\%$ and $\alpha_{WG} = 42\,\mathrm{cm}^{-1}$, as well as the measured points. In the calculation, a transparent carrier density of $N_g = 1.5 \times 10^{18}\,\mathrm{cm}^{-3}$, a differential gain of $\partial g/\partial N = 6.0 \times 10^{-16}\,\mathrm{cm}^2$, and a recombination coefficient of $B_{eff} = 1.5 \times 10^{-10}\,\mathrm{cm}^3/\mathrm{s}$ were used.[22] A surface grating structure[23] with a 30-nm depth, which produces an index-coupling coefficient of $\kappa_i = 1300\,\mathrm{cm}^{-1}$, was assumed. We can observe that the trend of the measured values is close to the theoretical curve of the FP lasers, even though there is larger scattering between $L = 450$–$500\,\mu\mathrm{m}$. As for the theoretical threshold current of the LCI-membrane DFB lasers, a minimum value of 0.3 mA is attainable with a cavity length of approximately 70 μm, in spite of the large waveguide loss of $42\,\mathrm{cm}^{-1}$, because it is significantly lower than the index-coupling coefficient ($1300\,\mathrm{cm}^{-1}$), and the effective reflectivity of the grating is not significantly affected.

Figure 6 shows the lasing spectrum of an LCI membrane laser at a bias current of twice the threshold. The cavity length and the stripe width were 370 and 0.7 μm, respectively. The resonant mode spacing or the free spectral range (FSR) was measured to be 0.87 nm, and the effective refractive index, n_{eff}, was found to be 3.8 from the following expression

$$\mathrm{FSR} \approx \frac{\lambda^2}{2n_{eff}L}. \quad (2)$$

From a calculation using the finite differential method, the equivalent refractive index, n_{eq}, of this device structure is estimated to be 2.6. Hence, the effective refractive index, n_{eff}, is approximately 3.0, using the popular wavelength dispersion of the refractive index $\partial n/\partial\lambda = -0.25\,\mu\mathrm{m}^{-1}$ for GaInAsP/InP lasers emitting at a wavelength of 1.5–1.6 μm. The same value was obtained for several other devices on the same bar. The reason for this discrepancy has not been explained to date, but it can be clarified by measuring the stopbands of DFB structures with a range of grating periods.

In conclusion, we first demonstrated RT-CW operation of an LCI membrane FP laser on a Si substrate with BCB adhesive bonding. A threshold current of as low as 2.5 mA and an external differential quantum efficiency of 44% were obtained for a device with a stripe width of 0.7 μm and a cavity length of 350 μm. From the cavity length dependence of the differential quantum efficiency, the internal quantum efficiency and the waveguide loss were found to be 75% and $42\,\mathrm{cm}^{-1}$, respectively. These results indicate that the lateral current injection into the thin membrane core structure is not degraded by nonradiative surface recombination, while the membrane structure is susceptible to large scattering loss caused by sidewall roughness. The obtained theoretical curve shows that a short cavity DFB laser with a strong index-coupling coefficient leads to very low threshold current operation. Hence, this design is a good candidate for an ultralow-power-consumption laser for on-chip optical interconnections.

Acknowledgments The authors would like to thank Professors M. Asada, Y. Miyamoto, T. Mizumoto, and S. Akiba of the Tokyo Institute of Technology, Tokyo, Japan, for fruitful discussions and comments. This work was supported by JSPS KAKENHI grants: numbers 24246061, 25709026, 25420321, and 13J08092.

1) M. J. Kobrinsky, B. A. Block, J.-F. Zheng, B. C. Barnett, E. Mohammed, M. Reshotko, F. Robertson, S. List, I. Young, and K. Cadien, Intel Technol. J. **8**, 129 (2004).
2) M. Haurylau, G. Chen, H. Chen, J. Zhang, N. A. Nelson, D. H. Albonesi, E. G. Friedman, and P. M. Fauchet, IEEE J. Sel. Top. Quantum Electron. **12**, 1699 (2006).

3) K. Ohashi, K. Nishi, T. Shimizu, M. Nakada, J. Fujikata, J. Ushida, S. Torii, K. Nose, M. Mizuno, H. Yukawa, M. Kinoshita, N. Suzuki, A. Gomyo, T. Ishi, D. Okamoto, K. Furue, T. Ueno, T. Tsuchizawa, T. Watanabe, K. Yamada, S. Itabashi, and J. Akedo, Proc. IEEE **97**, 1186 (2009).
4) B. Davari, R. H. Dennard, and G. G. Shahidi, Proc. IEEE **83**, 595 (1995).
5) D. A. B. Miller, Proc. IEEE **97**, 1166 (2009).
6) P. Moser, W. Hofmann, P. Wolf, J. A. Lott, G. Larisch, A. Payusov, N. N. Ledentsov, and D. Bimberg, Appl. Phys. Lett. **98**, 231106 (2011).
7) S. Imai, K. Takaki, S. Kamiya, H. Shimizu, J. Yoshida, Y. Kawakita, T. Takagi, K. Hiraiwa, H. Shimizu, T. Suzuki, N. Iwai, T. Ishikawa, N. Tsukiji, and A. Kasukawa, IEEE J. Sel. Top. Quantum Electron. **17**, 1614 (2011).
8) S. Matsuo, A. Shinya, T. Kakitsuka, K. Nozaki, T. Segawa, T. Sato, and M. Notomi, Nat. Photonics **4**, 648 (2010).
9) B. Ellis, M. A. Mayer, G. Shambat, T. Sarmiento, J. Harris, E. E. Haller, and J. Vuckovic, Nat. Photonics **5**, 297 (2011).
10) S. Matsuo, T. Sato, K. Takeda, A. Shinya, K. Nozaki, H. Taniyama, M. Notomi, K. Hasebe, and T. Kakitsuka, IEEE J. Sel. Top. Quantum Electron. **19**, 4900311 (2013).
11) T. Okamoto, N. Nunoya, Y. Onodera, S. Tamura, and S. Arai, Electron. Lett. **38**, 1444 (2002).
12) T. Okamoto, N. Nunoya, Y. Onodera, T. Yamazaki, S. Tamura, and S. Arai, IEEE J. Sel. Top. Quantum Electron. **9**, 1361 (2003).
13) T. Okamoto, T. Yamazaki, S. Sakamoto, S. Tamura, and S. Arai, IEEE Photonics Technol. Lett. **16**, 1242 (2004).
14) S. Sakamoto, H. Naitoh, M. Ohtake, Y. Nishimoto, T. Maruyama, N. Nishiyama, and S. Arai, Jpn. J. Appl. Phys. **46**, L1155 (2007).
15) T. Okumura, T. Koguchi, H. Ito, N. Nishiyama, and S. Arai, Appl. Phys. Express **4**, 042101 (2011).
16) S. Arai, N. Nishiyama, T. Maruyama, and T. Okumura, IEEE J. Sel. Top. Quantum Electron. **17**, 1381 (2011).
17) S. Sakamoto, H. Naitoh, M. Ohtake, Y. Nishimoto, S. Tamura, T. Maruyama, N. Nishiyama, and S. Arai, IEEE J. Sel. Top. Quantum Electron. **13**, 1135 (2007).
18) K. Oe, Y. Noguchi, and C. Caneau, IEEE Photonics Technol. Lett. **6**, 479 (1994).
19) M. Futami, K. Shinno, T. Shindo, K. Doi, T. Amemiya, N. Nishiyama, and S. Arai, Proc. 1st Opt. Interconnects Conf., 2012, p. 34.
20) K. Tanabe, T. Rae, K. Watanabe, and Y. Arakawa, Appl. Phys. Express **6**, 082703 (2013).
21) K. Doi, T. Shindo, M. Futami, J. Lee, T. Hiratani, D. Inoue, S. Yang, T. Amemiya, N. Nishiyama, and S. Arai, 25th Int. Conf. Indium Phosphide and Related Materials, 2013, p. 1.
22) T. Shindo, M. Futami, K. Doi, T. Amemiya, N. Nishiyama, and S. Arai, IEEE J. Sel. Top. Quantum Electron. **19**, 1502009 (2013).
23) T. Shindo, T. Okumura, H. Ito, T. Koguchi, D. Takahashi, Y. Atsumi, J. Kang, R. Osabe, T. Amemiya, N. Nishiyama, and S. Arai, Opt. Express **19**, 1884 (2011).